THE JOURNAL OF PHYSICAL CHEMISTRY C
A JOURNAL OF THE AMERICAN CHEMICAL SOCIETY

pubs.acs.org/JPCC

Article

Thickness-Dependent Raman Scattering from Thin-Film Systems

Nathan Van Velson,* Hamidreza Zobeiri, and Xinwei Wang*

Cite This: J. Phys. Chem. C 2023, 127, 2995−3004

Read Online

ACCESS | Metrics & More | Article Recommendations | Supporting Information

Downloaded via IOWA STATE UNIV on February 21, 2023 at 21:46:03 (UTC).
See https://pubs.acs.org/sharingguidelines for options on how to legitimately share published articles.

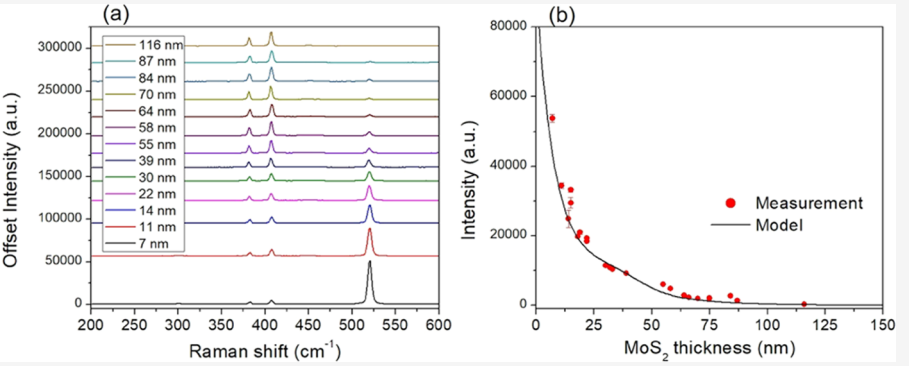

ABSTRACT: The intensity of the Raman signal from a thin-film multilayer varies nonmonotonically with the thickness of the thin-film layers due to interference of the excitation and Raman scattered light within the films. This phenomenon can be used to not only enhance the Raman signal but also investigate thin-film thickness and optical properties. Here, we perform an experimental study of the thickness dependence of the Raman signal from several thin-film material systems, including silicon-on-sapphire (SOS) and silicon nitride on SOS thin films, and multilayer MoS_2 prepared on silicon substrates. The measured intensities appropriately scaled are compared to an analytical model developed from the transfer matrix method. A good fit is found for the SOS thin films when the laser spot size is sufficiently larger than the film thickness. For the multilayer MoS_2, an excellent fit is found for the intensity of the Raman signal from the underlying Si substrate, while the intensity of the MoS_2 characteristic Raman shifts is impacted by laser parameters and sample orientation. These results have implications for thin-film metrology and optical properties characterization.

1. INTRODUCTION

Common techniques for determining the thickness of thin-film materials include optical methods such as reflectance spectroscopy[1] and ellipsometry.[2] In some cases, such as when the substrate on which the thin films are grown is transparent, these optical techniques can prove challenging and not provide accurate results. Silicon-on-sapphire (SOS) thin films are one example. For atomically thin two-dimensional (2D) materials, which have generated significant research interest recently, atomic force microscopy (AFM) is commonly employed for thickness measurement. However, AFM is time-consuming and gives only a relative difference in thickness between locations. Optical contrast is also a powerful tool for characterizing the number of layers of multilayer 2D materials such as graphene[3,4] and transition-metal dichalcogenides (TMDs).[5,6] However, optical contrast methods are limited to very few (<10−15) layers[4] and may result in artificial thicknesses due to interference.

Raman spectroscopy is an optical spectroscopy technique based on the inelastic scattering of light by vibrational modes of materials and is commonly used to characterize thin film and atomic layer materials.[7] Raman spectroscopy is employed in physical chemistry for fingerprinting materials,[8] probing structure and crystallinity,[9] noncontact temperature measurements,[10] and characterization of thermal energy transport,[11−13] among many other applications. While the Raman signature of each Raman-active material is unique, the intensity of the Raman signal depends on both sampling volume—the volume of material with which the excitation light interacts—and instrument parameters such as excitation laser frequency and intensity, detector efficiency and gain, and measurement integration time. If these experimental parameters are kept consistent between measurements, the intensity of the Raman signal from a thin-film sample could potentially be used as a measure of the film thickness.

Beginning in the 1980s, it has been shown the thickness of the layers in a multilayer thin film can have a large effect on the intensity of the Raman signal.[14,15] An enhancement of the measured Raman intensity was found at certain film thickness

Received: September 8, 2022
Revised: January 20, 2023
Published: February 3, 2023

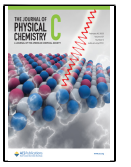

ACS Publications
© 2023 American Chemical Society

and has been shown to be due to interference of both the incident light as well as the Raman scattered light from multiple reflections at the thin film interfaces.[16−20] This interference-enhanced Raman scattering (IERS) phenomenon was used to maximize the Raman signal from very thin layers on top of a thicker layer, which was deposited on a substrate. In one case, the concept was used to determine an optimum excitation wavelength for enhancing the Raman signal.[18] Several of these studies have calculated the Raman signal intensity vs. thickness for one- or two-layer films on a semi-infinite substrate from the Fresnel equations with multiple-wave analysis.[16,17,19,21,22] Since the first demonstration of Raman enhancement of graphene on Si substrates with a SiO_2 capping layer (SiO_2/Si),[21,22] several researchers have used Raman intensity ratios to estimate the thicknesses of graphene,[23,24] MoS_2,[25] or hexagonal boron nitride[26] deposited on SiO_2/Si. These thickness or layer number estimations used the ratio of sample to substrate Raman intensities, or the ratio of substrate Raman intensity with the sample to bare substrate, and predicted these ratios based on either multiple-wave analysis or versions of the transfer matrix method (TMM). However, in multilayer films in which the substrate is not Raman-active, or there is otherwise only one Raman-active material in the structure, an intensity ratio would not be able to be used for thickness estimation. Solonenko et al. used a transfer matrix approach to calculate the enhancement of the Raman signal from F_{16}CuPc films on SiO_2/Si.[20] However, in their model, they neglected the thickness of the Raman-active layer, as well as the difference in wavelength between the incident and Raman scattered light. While these previous models gave some agreement with experimental results, a general solution for calculating the Raman signal intensity as a function of thickness for thin films with an arbitrary number of layers has not been reported.

In a previous work, we developed a rigorous treatment of the Raman signal from multilayer thin films using a transfer matrix method (TMM) approach.[27] This new physical model correctly accounts for the generation of the Raman signal within the film, and its propagation through the multilayer. The model is very versatile and can be applied to any multilayer thin film with an arbitrary number of layers. In this paper, we report on the experimental investigation of the thickness dependence of Raman intensity with thin film thickness for comparison to the previously developed TMM-based model. In Section 2, a brief overview of the TMM-based model is presented. Section 3 describes the experimental setup used in the experimental investigation, while results for sub-micron semiconductor thin films (silicon-on-sapphire) and multilayer MoS_2 are presented in Sections 4 and 5, respectively. The potential for application of these results to thin-film metrology and optical properties measurement is also discussed.

2. RAMAN INTENSITY FROM MULTILAYER FILMS

The intensity of the Raman signal from an individual layer within a multilayer thin-film system can be determined from an extension of the transmission matrix method (TMM) for light propagation through thin films. The TMM takes into account the multiple reflections of the incident light off each of the thin-film interfaces to determine the overall reflection and transmission of the multilayer.[28] The electric field intensity due to the incident excitation light can also be determined at each location within the thin-film layer of interest using the TMM. Consider a multilayer thin-film system as shown in Figure 1. The electric field amplitude in the positive and negative

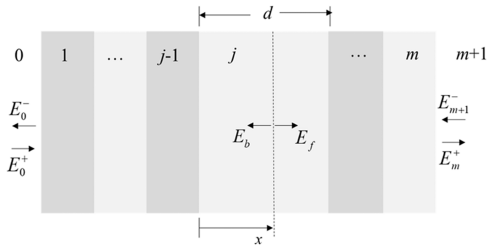

Figure 1. Multilayer thin-film system with m layers and Raman-active layer j with thickness d. The electric field intensity of the incident excitation light can be computed from the transfer matrix method (TMM) at any location x within layer j. The resulting Raman signal generated at location x has a forward propagating component E_f and a backward propagating component E_b. The TMM can be used to determine the total intensity of the measured Raman signal as a function of layer j thickness.

directions at the front and back surfaces of the multilayer are determined by the transfer matrix S

$$\begin{pmatrix} E_0^+ \\ E_0^- \end{pmatrix} = S \begin{pmatrix} E_{m+1}^+ \\ E_{m+1}^- \end{pmatrix} \tag{1}$$

The transfer matrix S is the matrix product of an interface matrix for each interface between layers and a propagation matrix for each layer. For a layer j, the transfer matrix can be written as $S = U_j L_j D_j$, where U_j is the partial transfer matrix for the layers before layer j, D_j is the partial transfer matrix for the layers after layer j, and L_j is the propagation matrix for the layer j. When these matrices are known, the electric field amplitude at a position x within layer j is calculated as

$$E_j(x) = [(D_{j11}/S_{j11})e^{-i\beta_j(d_j - x)} + (D_{j21}/S_{j11})e^{i\beta_j(d_j - x)}]E_0^+ \tag{2}$$

where $\beta_j = (2\pi/\lambda)n_j$.

The propagation of the Raman signal generated at a location within the multilayer thin film to the surface of the multilayer where it can be measured may also be determined using a TMM-based approach. The details of this calculation are given in our previous work by Van Velson et al.[27] The Raman signal generated at a location x within layer j is assumed to have two components, one that propagates in the forward direction and one that propagates in the backward direction. The TMM is applied to each to determine the amplitude of the light at the surface of the multilayer, $E_{0,f}$ and $E_{0,b}$ for the forward and backward propagating Raman signals, respectively. In addition to the multiple reflections off each interface of the Raman light, the model is the first to correctly account for the generation of the Raman signal by including a discontinuity at the point of the Raman signal generation.

The intensity of the Raman light generated at a given location within the multilayer thin film is proportional to the electric field intensity of the incident light at the location. Assuming the forward and backward propagating Raman signals are incoherent, the values of the respective Raman light electric field intensities at the surface of the multifilm are summed together, and the sum weighted by the incident light electric field intensity. This is then integrated over the

https://doi.org/10.1021/acs.jpcc.2c06353
J. Phys. Chem. C 2023, 127, 2995−3004

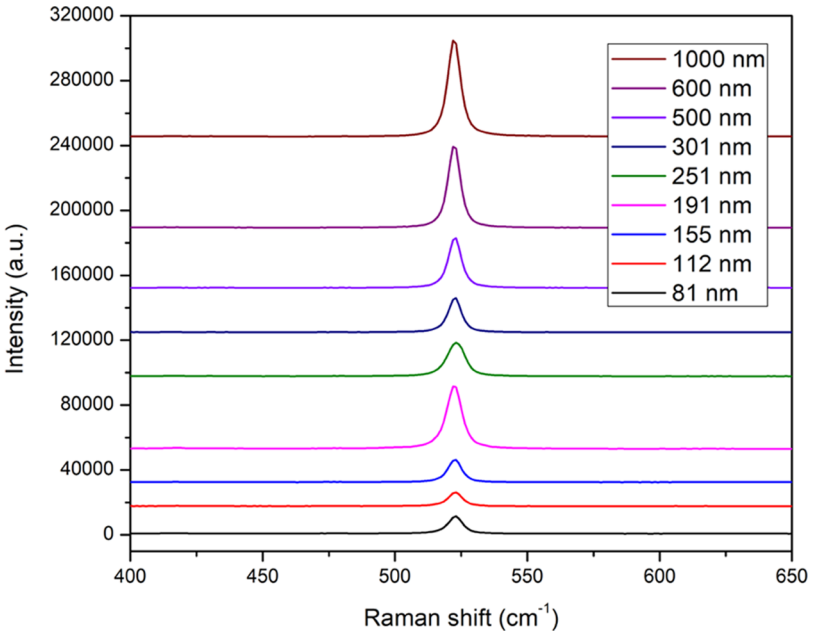

Figure 2. Raman spectra obtained from silicon-on-sapphire thin films acquired with 532 nm excitation laser and 100× microscope objective. Note the nonmonotonic trend of intensity with thickness.

thickness of the Raman-active layer to obtain the total Raman signal intensity:

$$I_{\text{Raman}} = \int_j [|E_j(x)|^2 \cdot (|E_{0,b}^-|^2 + |E_{0,f}^-|^2)]\mathrm{d}x \quad (3)$$

As has been previously shown,[21,22] the trend of Raman intensity is not monotonic with thickness due to the interference of the reflections off the various thin-film interfaces. In practice, the measured Raman intensity from a sample is reported in "arbitrary units" or "counts" as there are many instrument factors such as excitation laser intensity, optical throughput, detector efficiency and gain, etc., that influence the reported intensity. However, for a given instrument, if these experimental parameters are carefully controlled, the above method may be used for predicting the measured Raman intensity as a function of thin film thickness. An instrument-specific scaling factor (SF) may then be applied for comparison of the above model with measured intensities. The use of an instrument scaling factor is a way to normalize the measured intensity to the model predictions. The model results are scaled proportionally to fit the number of counts recorded by the detector (i.e., the intensity), which is arbitrary and depends on instrument parameters. Similarly, an "enhancement factor" can be employed, which is another way of normalizing the results.

3. EXPERIMENTAL SETUP

The Raman measurements were performed in a backscattered Raman spectrometer setup equipped with 532 nm and 785 nm excitation lasers. The 532 nm laser is directly coupled to the microscope optics, while the 785 nm laser is fiber-coupled. Free-space optics direct the laser light to the optical microscope (Olympus BX-53), which is equipped with 10× (NA = 0.30), 50× (NA = 0.50), and 100× objectives (NA = 0.80). Typically, the 100× objective is used, which results in a laser spot on the sample of less than 1 μm in diameter for the 532 nm laser. Two neutral density filters allow the laser intensity to be reduced by 10× or 100×, respectively. The spectrometer (Horiba iHR 320) utilizes an 1800 g/mm diffraction grating and a TEC-cooled CCD detector (Horiba Syncerity). Measurement parameters including laser intensity, inlet slit width, and integration time are held constant between individual measurements of the same sample set. Individual Raman peaks in the measured spectra are fit to a Lorentzian profile to obtain a value for the signal intensity. A three-dimensional (3D) micro-stage is used to position the sample in the x- and y-directions, and to adjust the sample in the z-direction for focusing of the laser onto the sample surface. The laser is focused onto the sample by evaluating the laser spot through the microscope.

4. SUB-MICRON MATERIAL THICKNESS INVESTIGATION

4.1. Silicon-on-Sapphire. Six silicon-on-sapphire (SOS) samples were prepared from commercially available 500 nm thick epitaxial Si grown on 5 mm square sapphire substrates (www.mtixtl.com). Dry chemical etching was used to reduce the thickness of the Si layer. The starting and final thicknesses were estimated by ellipsometry and found to be in the range of 80−300 nm. The estimated uncertainty in the measured thicknesses is 5%, based on variations in measured Raman intensities across each sample. Three additional samples with reported thicknesses of 500, 600, and 1000 nm were also purchased and used as received. Three Raman spectra were collected from each of the SOS samples using the 532 nm excitation laser. The laser power was 50 mW, and the measurement integration time was 1 s. The spectrometer inlet slit width was set at 200 μm. Example spectra from each sample are shown in Figure 2. The measurements were then repeated with the 785 nm excitation laser. With the 785 nm laser, the laser power is 350 mW, with a measurement integration time of 5 s. The spectrometer inlet slit width was set to 1 mm. For the above measurements, the 100× microscope objective was used.

For comparison of the intensities of the measured Raman spectra to the TMM-based model described above, the

https://doi.org/10.1021/acs.jpcc.2c06353
J. Phys. Chem. C 2023, 127, 2995−3004

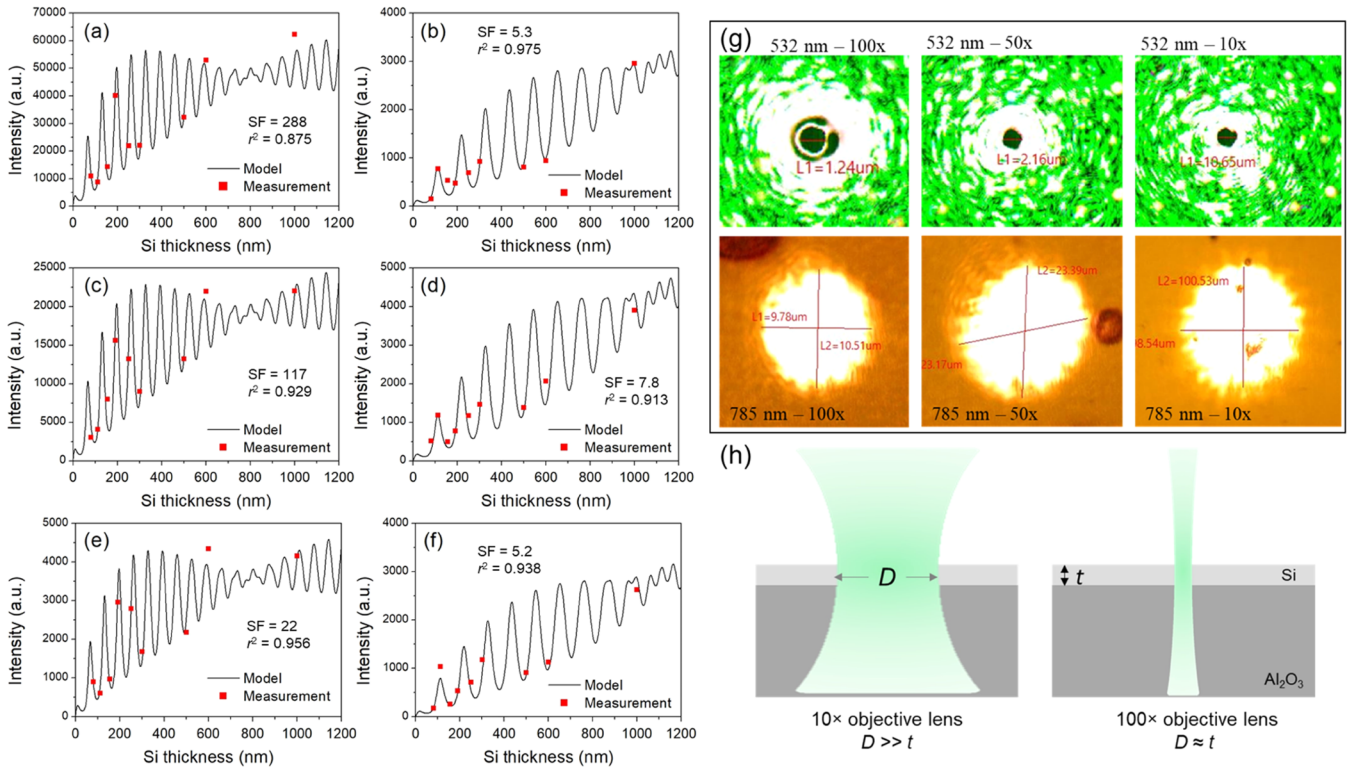

Figure 3. Comparison of predicted to measured Raman intensity of the 521 cm^{-1} Si peak for silicon-on-sapphire thin films for (a) 100× objective, 532 nm laser [scaling factor (SF) = 288, r^2 = 0.875]; (b) 100× objective, 785 nm laser (SF = 5.3, r^2 = 0.975); (c) 50× objective, 532 nm laser (SF = 117, r^2 = 0.929); (d) 50× objective, 785 nm laser (SF = 7.8, r^2 = 0.913); (e) 10× objective, 532 nm laser (SF = 22, r^2 = 0.956); (f) 10× objective, 785 nm laser (SF = 5.2, r^2 = 0.938). Instrument scaling factor determined by least-squares fitting. (g) Measured diameters of 532 and 785 nm focused laser with 100×, 50×, and 10× microscope objective lenses. (h) Illustration of the relation of incident laser beam waist to film thickness on the validity of the model assumption of a normally incident plane wave.

predicted intensities must be appropriately scaled for the Raman spectrometer setup and set of parameters used in the measurements. The mean fitted intensity of the 521 cm^{-1} Si Raman peak is determined for each sample, and a least-squares fitting is performed to determine the scaling factor that provides the best fit of the scaled predicted values with the measured intensities. For the measurements taken with the 532 nm laser and associated parameters, the fitted scaling factor was found to be 288 (r^2 = 0.875). For the 785 nm laser, the fitted scaling factor was 5.3 (r^2 = 0.975). The measured Raman intensities are compared to the model for both excitation lasers in Figure 3a,b.

Observing the results obtained with the 532 nm laser, the measured Raman intensities are predicted well by the scaled model at thicknesses below 500 nm, while the measured intensities for the 600 and 1000 nm samples are somewhat higher than the predicted values. This may be due to a higher level of crystallinity than the etched samples, resulting in a stronger Raman signal or a difference in the index of refraction. However, it is more likely due to the thicknesses of these two samples and the assumptions used in the multilayer thin film Raman intensity model. A simplifying assumption in the model is that the excitation light consists of a normally incident plane wave. When the film thickness is small compared to the diameter of the focused laser on the sample surface, and correspondingly the focal depth of the laser, this is a valid assumption, as the majority of light in a Gaussian beam is approximately normally incident.[25] However, when the thickness of the sample is on the same order or larger than the laser spot, then this assumption is violated (Figure 3h). For improved fit of the data over a larger thickness range, the model would have to be modified to consider the numerical aperture (NA) of the microscope objective by also integrating over the incident angle and treating separately the s- and p-polarized components.[24] However, for most semiconductor device fabrication, Si film thicknesses larger than 500 nm would likely not be encountered, and the normally incident assumption is accurate enough. In the present Raman spectrometer setup, when using the 100× objective with the 532 nm laser, the laser spot size is around 1 μm, on the order of the largest silicon film thickness. By contrast, the 785 nm laser with the 100× objective has a spot size of around 10 μm. The laser spot size measured on the surface of the sample is shown in Figure 3g for both lasers and all three available microscope objectives. The 785 nm laser spot size is disproportionately larger than the 532 nm laser because it is coupled to the Raman system by an optical fiber, which results in a loss of spatial coherence, while the 532 nm laser is directly coupled to the system.

The Raman measurements of the SOS thin films were repeated using the 50× and 10× microscope objectives. The scaling factor determined by least-squares fitting for the 50× objective is 117 (r^2 = 0.929) for the 532 nm laser and 7.8 (r^2 = 0.913) for the 785 nm laser. With the 50× objective, the 532 nm laser spot size is around 2 μm in diameter, while the 785 nm laser spot size is roughly 23 μm. Note that the integration time was increased to 10 s for the 785 nm laser Raman measurements. The comparisons of the measured Raman peak

https://doi.org/10.1021/acs.jpcc.2c06353
J. Phys. Chem. C 2023, 127, 2995−3004

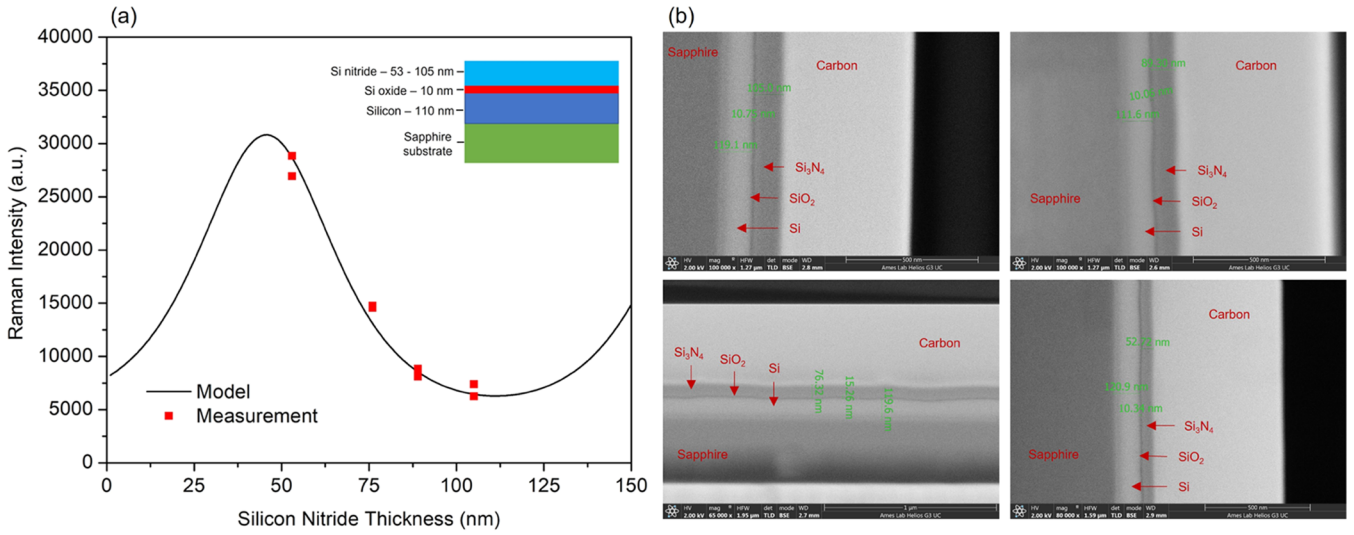

Figure 4. (a) Comparison of predicted and measured intensity of the 521 cm^{-1} Si Raman peak from the silicon nitride on SOS samples. Measurements taken with 532 nm laser and 100× microscope objective. Instrument scaling factor determined by least-squares fitting. Inset: Silicon nitride on SOS thin-film structure. (b) SEM images of sample cross sections prepared by FIB lithography to determine the thickness of silicon nitride layer in etched thin-film samples.

intensities to the scaled model predictions for the 50× objective are given in Figure 3c,d. Finally, the results obtained with the 10× objective are shown in Figure 3e,f. With this objective, the 532 nm laser spot size is around 10 μm, while the 785 nm laser spot size is around 100 μm. The scaling factor for the 532 nm laser is determined by least-squares fitting to be 22 (r^2 = 0.956), while the scaling factor for the 785 nm laser is determined to be 5.2 (r^2 = 0.938).

As indicated by the improved goodness of fit (r^2) of the fitted scaling factor with decreasing microscope objective power for the 532 nm measurements, the larger laser spot size does improve the agreement between measurement and model, and extends the application of the model to larger thin-film thicknesses. For the measurements with the 785 nm laser, there is not as substantial an improvement in the fitting with lower power objectives, due to the large laser spot size even with the 100× objective. Larger laser spot sizes also have the effect of smoothing out the impacts of surface roughness and local variations in film thickness. There is therefore a trade-off between using lower or higher-power microscope objectives, especially for the 532 nm laser. Higher-power objectives result in higher measured intensities and signal-to-noise ratios, as well as higher spatial resolution, but can result in conditions where model assumptions are violated. Meanwhile, lower power objectives extend the range of thicknesses at which the model is applicable, at the expense of lower signal-to-noise ratio and spatial resolution. Finally, using a least-squares fitting is useful for determining the instrument-specific scaling factor when a large number of samples with known thicknesses are available. However, for applications in thin-film metrology, it would be useful to be able to calibrate the scaling factor for a given Raman spectrometer setup with a small number of known samples, which can have an impact on the selection of microscope objective used.

4.2. Silicon Nitride on SOS. An additional set of samples was prepared from an existing silicon-on-sapphire wafer on which an approximately 10 nm silicon oxide layer was grown over a 110 nm Si layer. Above the oxide layer is a silicon nitride layer with an initial thickness of approximately 140 nm. Eight samples were prepared by etching pieces of the wafer in a phosphoric acid bath to reduce the thickness of the nitride layer. The thicknesses of the nitride layers were confirmed using focused ion beam (FIB) lithography to etch a cross section of the layers, which was then imaged with scanning electron microscopy (SEM) to determine the thickness. The nitride layer thicknesses were determined to be 53, 76, 89, and 105 nm, with an uncertainty of approximately 5 nm based on the resolution of the SEM images. Two samples were prepared for each thickness. SEM images of the sample cross section are given in Figure 4b.

This then becomes a five-layer thin-film structure (air/Si_3N_4/SiO_2/Si/sapphire) to which the TMM approach can be applied. In the following measurements, the change in the Raman intensity from the Si layer as the silicon nitride layer thickness changes was evaluated. Three Raman spectra were taken from each silicon nitride sample with the 532 nm laser. Again, the laser power was 50 mW, the integration time was 1 s, and the inlet slit width was set at 200 μm. A least-squares fitting was again used to determine the instrument scaling factor that best fit the measured intensities of the 521 cm^{-1} Si Raman peak from each sample. While the thickness of the silicon nitride layer is varied, the Raman signal from the underlying Si layer is much stronger than any potential Raman signature from the nitride layer and is thus used as a measure of the thickness of the nitride layer. The scaling factor was found to have a value of 237 for the instrument and parameters used. A comparison of the measured Si peak intensities to the scaled model is shown in Figure 4a.

In the calculation of the predicted Si Raman intensity, the thicknesses of the silicon oxide and silicon layers are inputs to the model in addition to the nitride layer thickness. These were fixed at 10 and 110 nm for the oxide and Si layers, respectively. However, other combinations of Si and oxide layer thicknesses may also provide good fittings of the data, with new scaling factors for these values. This opens up the possibility of doing a multivariable least-squares fitting to determine the thickness of more than one layer in a multilayer thin-film stack. Measure-

https://doi.org/10.1021/acs.jpcc.2c06353
J. Phys. Chem. C 2023, 127, 2995−3004

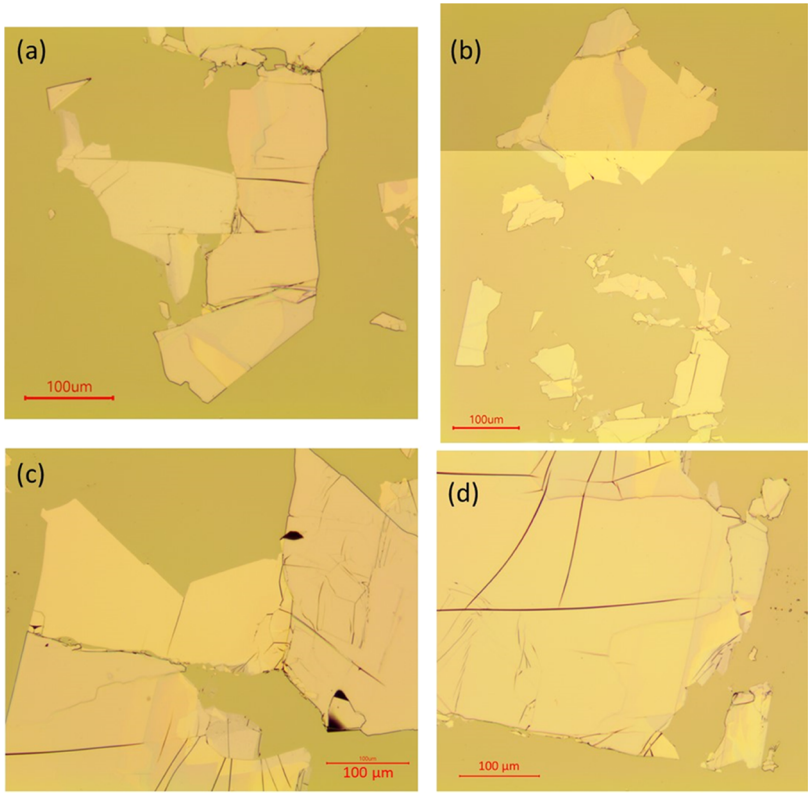

Figure 5. Optical images of three samples of MoS_2 prepared on a Si substrate. Imaged with a 10× microscope objective. (a) Sample 1—MoS_2 multilayer thicknesses of 15−116 nm. AFM measurement locations and results shown in Supporting Information Figures S1 and S2. (b) Sample 2—MoS_2 multilayer thicknesses of 33−87 nm. AFM measurement locations and results shown in Supporting Information Figure S3. (c, d) Two regions of Sample 3—MoS_2 multilayer thicknesses of 7−66 nm. AFM measurement locations and results shown in Supporting Information Figure S4.

ments at a larger number of thicknesses would be needed to improve the data fitting.

5. ATOMIC LAYER 2D MATERIAL THICKNESS INVESTIGATION

5.1. Sample Preparation. Many-layer MoS_2 samples were prepared directly on a Si substrate using the mechanical exfoliation method.[29] Here, MoS_2 layers are peeled from the bulk material using adhesive tape. The MoS_2 layers are transferred to a gel film. The gel film is brought in contact with the Si substrate and slowly removed, leaving the MoS_2 layers attached to the Si surface. Three separate deposited samples were identified by optical microscopy and then characterized with atomic force microscopy (AFM) (NMAFM-2, Digital Instruments). Previous measurements have shown multilayer MoS_2 to have a surface roughness of around 1 nm.[30] Seven locations on the first sample were found by AFM to have thicknesses between 15 and 116 nm. Five locations measured on the second sample were determined to have thicknesses between 33 and 87 nm. Finally, the MoS_2 layers in the third sample were found to have thicknesses between 7 and 66 nm at the six locations measured by AFM. Optical images of the three samples are shown in Figure 5. Higher-magnification images of the three samples and AFM measurement locations are given in Supporting Information Figures S1−S4.

5.2. MoS_2 Raman Investigation. To investigate the thickness dependence of the Raman spectrum on the thickness of the MoS_2 layers, 10 Raman spectra were collected from each of the 24 locations on the three samples that were identified and measured with AFM, covering 20 different MoS_2 layer thicknesses with values ranging from 7 to 116 nm. These nonresonant Raman measurements were performed with a 532 nm laser. The laser power was 2 mW, the spectrometer inlet slit was set at 100 μm, and the 100× microscope objective was used. The integration time for each measurement was 30 s. A sampling of the Raman spectra acquired from these samples is provided in Figure 6a. The main features of the spectra are the 521 cm^{-1} peak from the underlying Si substrate, and the two MoS_2 Raman shifts at around 382 cm^{-1} (E^1_{2g}) and 408 cm^{-1} (A_{1g}).

The mean intensities of both the Si and MoS_2 Raman shifts measured at each thickness are compared to the intensities predicted using the TMM-based model with bulk MoS_2 optical properties.[31] The instrument scaling factor for each was again determined by a least-squares fitting that minimizes the difference between the scaled curve and the measured intensities. For the Si Raman signal, the scaling factor was found to be 893. For the 382 and 408 cm^{-1} Raman peaks, it was found to be 1858 and 3218, respectively. In Figure 6b−d, the measured intensities of each of the three Raman shifts in the spectrum of MoS_2 on Si are plotted against the scaled model. The intensity of the Si Raman signal is well predicted by the scaled model. In this case, the trend of signal intensity from the underlying substrate with MoS_2 thickness decreases monotonically, due to the increased absorption of the signal as the MoS_2 layer increases.

The trend of the two MoS_2 Raman shift intensities with thickness in Figure 6c,d are nearly identical, only shifted by

https://doi.org/10.1021/acs.jpcc.2c06353
J. Phys. Chem. C 2023, 127, 2995−3004

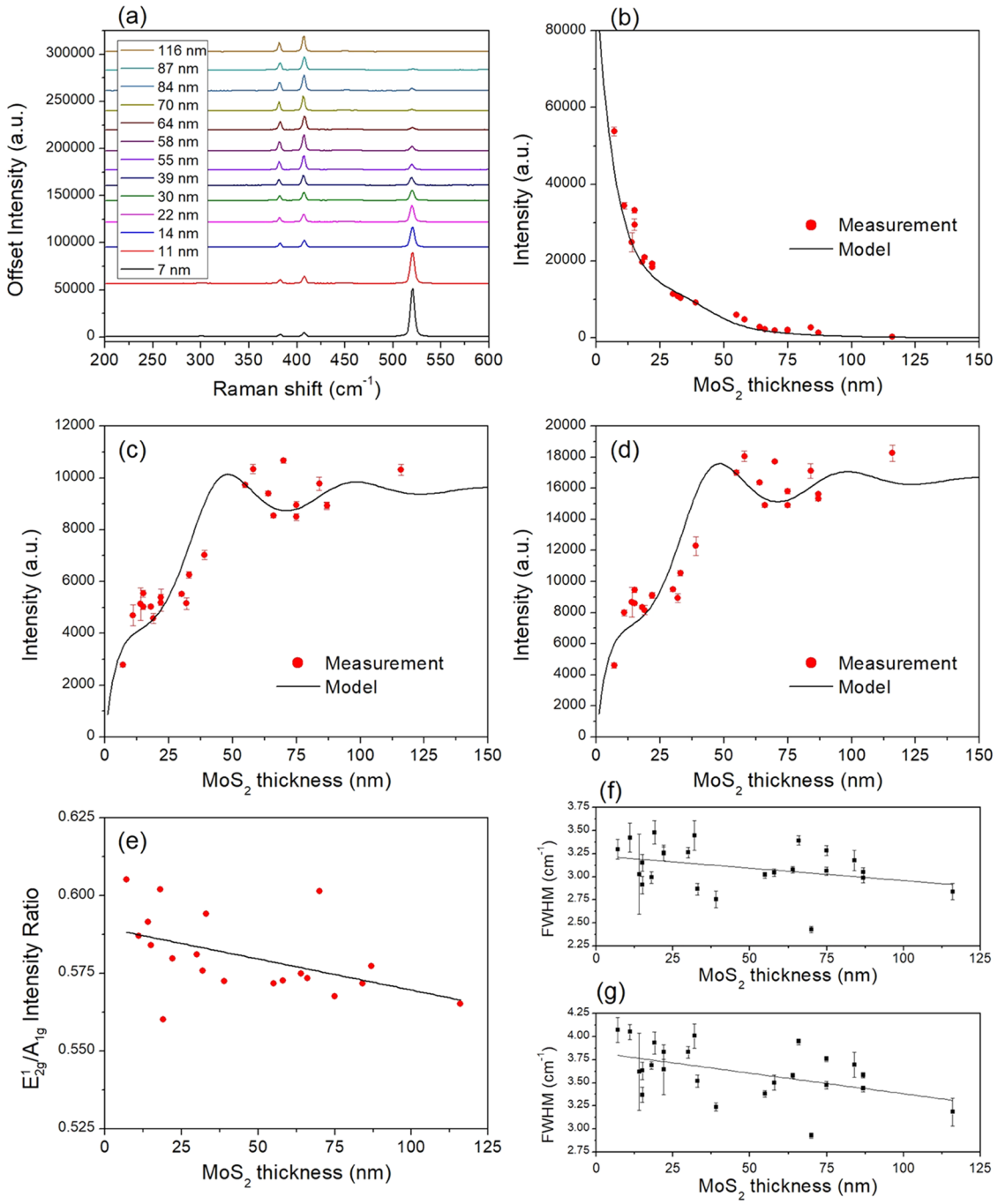

Figure 6. (a) Select Raman spectra obtained from MoS_2 layers prepared on Si substrate. (b–d) Comparison of predicted intensity against measured intensity of Raman peaks from spectra for of MoS_2 on Si for (b) 521 cm^{-1} Si Raman shift, (c) 382 cm^{-1} MoS_2 Raman shift, and (d) 408 cm^{-1} MoS_2 Raman shift. (e) Ratio of Raman signal intensity of $MoS_2E^1_{2g}$ to A_{1g} decreases with MoS_2 thickness. The solid line is a linear fit (r^2 = 0.23). (f) Average full width at half-maximum (FWHM) of $MoS_2E^1_{2g}$ peak at each measured location. (g) Average FWHM of MoS_2A_{1g} peak at each measured location. Solid lines in (f) and (g) are linear fits for illustration.

scale. This is to be expected if the ratio between the E^1_{2g} and A_{1g} peak intensities was constant. In reality, as shown in Figure 6e, the ratio between the peak intensities decreases somewhat with thickness, by 4–7%, though the correlation is not strong. This trend has also been seen in previous studies.[32] They reported an increase in the A_{1g}/E^1_{2g} intensity ratio for WS_2 with increasing number of layers up to five layers and a small increase in the intensity ratio from five layers to bulk WS_2. WS_2 is an isoelectronic compound of MoS_2 and should show similar behavior. Here, we report the inverse ratio (E^1_{2g}/A_{1g}). Therefore, the slight decrease in the ratio observed in our measurements is consistent with the literature. A weak correlation with thickness is also seen in the full width at half-maximum (FWHM) of the MoS_2 Raman peaks (Figure 6f,g). Though the decrease in FWHM is only on the order of 10%, this could be due to the increasing quality of the crystallinity as the MoS_2 layers increase toward bulk thickness. There was no discernable trend in the Raman shift peak location with thickness for the MoS_2 peaks. While the Raman peak location will red- or blue-shift for the E^1_{2g} or A_{1g} bands,

https://doi.org/10.1021/acs.jpcc.2c06353
J. Phys. Chem. C 2023, 127, 2995−3004

respectively, with increasing number of layers, after around 7–8 layers, the peak location is indistinguishable from that of the bulk material. For the present sample, even the smallest layer thickness of 7 nm corresponds to 8–9 layers.

In these measurements, the intensity of the A_{1g} Raman shift is higher than that of the E^1_{2g} shift. This is in contrast to other researchers who have reported MoS_2 Raman spectra in which the E^1_{2g} intensity is greater.[33,34] However, research performed by our lab with a different Raman spectrometer setup also reported A_{1g} peak intensities that are greater, as have others.[35,36] Liang et al. described how the ratio of intensities E^1_{2g}/A_{1g} is extremely sensitive to the polarization of the incident laser light.[37] The intensity ratio is additionally sensitive to the orientation of the MoS_2 layers and their stacking. This sensitivity to laser polarization and sample orientation can add significant variance to the measured intensity of the MoS_2 Raman signal. Due to this sensitivity, the effective scaling factor for a given set of instrument parameters can vary depending on sample orientation and stacking. This in turn explains the discrepancies between the measured intensities and the scaled model for the MoS_2 peaks, and why the fitting of the measured intensities for the Si Raman signal is much better.

To further illustrate the sensitivity of the E^1_{2g}/A_{1g} intensity ratio on the laser and spectrometer setup, consider the Raman spectra acquired using a 785 nm laser from arbitrary locations on the MoS_2 samples (Figure 7). Here, the laser power was

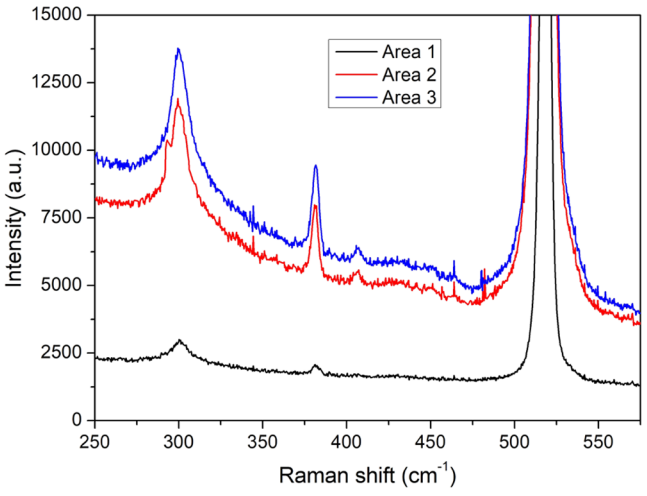

Figure 7. MoS_2 Raman spectra acquired with 785 nm laser; 60 s integration time (Area 1) and 240 s integration time (Areas 2 and 3). When using a nonpolarized excitation laser, the E^1_{2g}/A_{1g} intensity ratio is greater than 1.

350 mW and the spectrometer inlet slit was 1000 μm. The measurement integration time was 60 s (Area 1) or 240 s (Areas 2 and 3). With the lower-frequency incident light, the Raman signal is very weak compared to that of the underlying Si. In addition to the 521 cm^{-1} Si peak, the peak at 300 cm^{-1} that is visible is the 2TA(X) peak of the silicon substrate.[38] Here, the 785 nm laser is nonpolarized, with which the E^1_{2g} shift has a stronger intensity than the A_{1g} peak, and the intensity ratio is greater than 1.

6. DISCUSSION

As seen in the predicted Raman signal intensities for SOS thin films and MoS_2 on Si samples, the relation between the Raman intensity and film thickness is in general nonmonotonic with increasing thickness. However, due to the strong absorption of light within the MoS_2 layers, the intensity of the Raman signal from the underlying Si substrate does decrease monotonically with MoS_2 thickness. Therefore, it is possible to use the intensity of the 521 cm^{-1} Si Raman peak as an indicator of the thickness of the MoS_2 layers.

As a demonstration, Raman spectra were taken at one arbitrary location on each of the MoS_2 samples with unknown thickness (Figure 8a). The measurements were performed with the 532 nm laser and the same instrument parameters as previously. The intensity of the 521 cm^{-1} Si peak was compared to the scaled curve in Figure 6b. From an interpolation of this curve, the thickness of the three measured locations is estimated to be 46, 54, and 71 nm, respectively. As a check, the intensity of 382 cm^{-1} MoS_2 Raman shift from these measurements is compared to the scaled curve in Figure 6c at these estimated thicknesses (Figure 8b). The deviation from the scaled curve in Figure 8b is within 20%, similar to that in Figure 6c, and expected due to the arbitrary sample orientation with regard to laser polarization. This supports the use of the Raman signal from the underlying Si substrate as an indicator of MoS_2 thickness. In general, due to the non-monotonic trend of Raman intensity with layer thickness, a single Raman measurement would not be sufficient for a thickness estimation. However, two Raman intensities obtained with different excitation wavelengths would provide enough information to determine a sample thickness. The use of a scaled intensity as opposed to an intensity ratio also requires an a priori calibration of the scaling factor for the instrument to be used prior to determining the thickness of new samples.

In addition to potential application in thin-film metrology, the thickness dependence of the Raman signal from thin films can be used to investigate the optical properties of thin-film materials. For many two-dimensional materials, such as graphene and TMDs like MoS_2, the optical properties may not be well understood or have disagreement in the literature. The enhancement of the Raman signal from thin films is highly dependent on the complex index of refraction of the thin film and substrate materials. Among other things, the index of refraction determines the period and amplitude of the variation in the Raman intensity with thickness. If the thickness of a thin film sample or set of samples is known a priori, a Raman-based methodology could be developed to characterize the film's optical properties as an inverse problem, or to verify values obtained from other methods such as ellipsometry.

7. CONCLUSIONS

In this work, the thickness dependence of the Raman signal enhancement from thin films and multilayer thin-film systems is investigated. The intensity of the Raman shift from a given thin-film system is predicted from a transfer matrix method (TMM) based model and appropriately scaled for a specific experimental setup. The validity of this model was confirmed with Raman measurements of silicon-on-sapphire (SOS) thin films, and silicon nitride on SOS thin films. For SOS thin films, the TMM model is most valid when the thickness of the film is much less than the incident laser spot size and focal depth. Application of the TMM approach was further validated in the measurement of a five-layer thin-film structure (silicon nitride on SiO_2/SOS).

Similar measurements were performed on multilayer MoS_2 prepared on silicon substrates. The intensities of both the

https://doi.org/10.1021/acs.jpcc.2c06353
J. Phys. Chem. C 2023, 127, 2995–3004

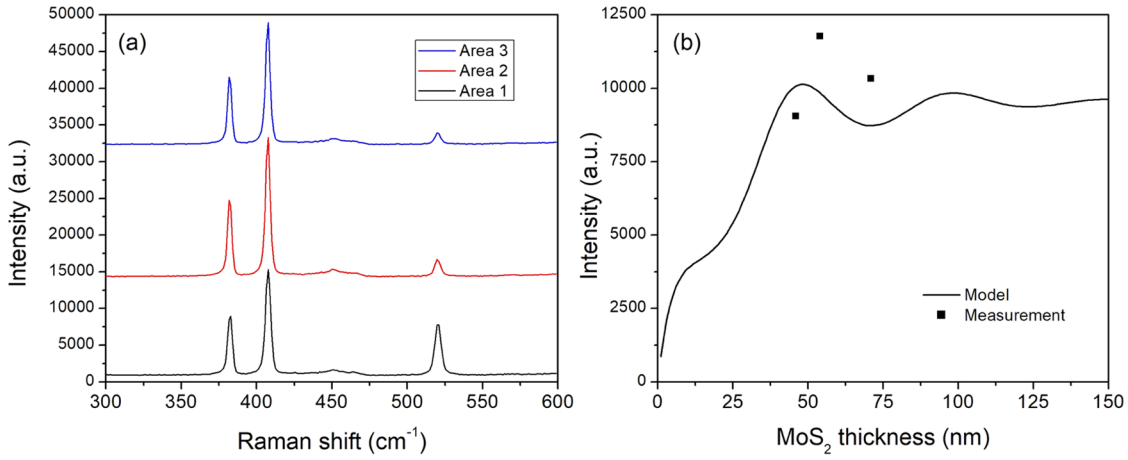

Figure 8. (a) Raman spectra measured at arbitrary locations on the three MoS_2 on Si samples as a demonstration of the potential use of the Si Raman signal intensity as an indicator of MoS_2 thickness. (b) Intensity of the 382 cm^{-1} MoS_2 Raman shift from three samples plotted at thicknesses estimated from the Si Raman shift intensity, alongside predicted intensity curve with previously determined scaling factor.

silicon Raman shift at 521 cm^{-1} and the two Raman peaks from MoS_2 were predicted from the TMM model. An excellent fitting of the measured intensity was found for the silicon Raman shift. The intensity of the MoS_2 Raman peaks followed the trend of the model but are impacted by the polarization of the incident laser relative to the sample orientation, as is the E^1_{2g}/A_{1g} intensity ratio. Even so, it was demonstrated how the intensity of the Raman signal from the underlying Si substrate can be used as a measure of the MoS_2 layer thickness. The results presented here have implications for novel thin-film metrology techniques, as well as probing of thin-film and two-dimensional material optical properties.

■ ASSOCIATED CONTENT

Supporting Information

The Supporting Information is available free of charge at https://pubs.acs.org/doi/10.1021/acs.jpcc.2c06353.

Optical images of multilayer MoS_2 on Si samples, with locations of AFM measurements indicated; AFM measurement images inset for each measurement location; regions on sample 1 with MoS_2 thicknesses between 15 and 116 nm identified; regions on sample 2 with MoS_2 thicknesses between 33 and 87 nm identified; and regions on sample 3 with MoS_2 thicknesses between 7 and 66 nm identified (PDF)

■ AUTHOR INFORMATION

Corresponding Authors

Nathan Van Velson − *Research and Development Department, Advanced Cooling Technologies, Inc., Lancaster, Pennsylvania 17601-5688, United States;* orcid.org/0000-0001-8458-3028; Email: Nathan.vanvelson@1-act.com

Xinwei Wang − *Department of Mechanical Engineering, Iowa State University, Ames, Iowa 50011, United States;* orcid.org/0000-0002-9373-3750; Email: xwang3@iastate.edu

Author

Hamidreza Zobeiri − *Department of Mechanical Engineering, Iowa State University, Ames, Iowa 50011, United States*

Complete contact information is available at: https://pubs.acs.org/10.1021/acs.jpcc.2c06353

Notes

The authors declare no competing financial interest.

■ ACKNOWLEDGMENTS

This work was supported by Defense Microelectronics Activity (HQ072718C0008) and National Science Foundation (CBET1930866).

■ REFERENCES

(1) Chabli, A. Optical characterization of layers for silicon microelectronics. *Microelectron. Eng.* **1998**, *40*, 263−274.

(2) Schroder, D. K.*Semiconductor Material and Device Characterization*; Wiley: Hoboken, NJ, USA, 2015.

(3) Blake, P.; Hill, E. W.; Neto, A. H. C.; Novoselov, D.; Jiang, D.; Yang, R.; Booth, T. J.; Geim, A. K. Making graphene visible. *Appl. Phys. Lett.* **2007**, *91*, No. 063124.

(4) Ni, Z. H.; Wang, H. M.; Kasin, J.; Fan, H. M.; Yu, T.; Wu, Y. H.; Feng, Y. P.; Shen, Z. X. Graphene thickness determination using reflection and contrast spectroscopy. *Nano Lett.* **2007**, *7*, 2758−2763.

(5) Li, H.; Wu, J.; Huang, X.; Lu, G.; Yang, J.; Lu, X.; Xiong, Q.; Zhang, H. Rapid and reliable thickness identification of two-dimensional nanosheets using optical microscopy. *ACS Nano* **2013**, *7*, 10344−10353.

(6) Anzai, Y.; Yamamoto, M.; Genchi, S.; Watanabe, K.; Taniguchi, T.; Ichikawa, S.; Fujiwara, Y.; Tanaka, H. Broad range thickness identification of hexagonal boron nitride by colors. *Appl. Phys. Express* **2019**, *12*, No. 055007.

(7) Smith, E.*Modern Raman spectroscopy: A Practical Approach/Ewen Smith, Geoffrey Dent*; Wiley: Hoboken, NJ, USA, 2019.

(8) Kudelski, A. Analytical applications of Raman spectroscopy. *Talanta* **2008**, *76*, 1−8.

(9) Malard, L. M.; Pimenta, M. A.; Dresselhaus, G.; Dresselhaus, M. S. Raman spectroscopy in graphene. *Phys. Rep.* **2009**, *473*, 51−87.

(10) Yue, Y.; Wang, X. Nanoscale thermal probing. *Nano Rev.* **2012**, *3*, 11586.

(11) Yue, Y.; Zhang, J.; Wang, X. Micro/Nanoscale Spatial Resolution Temperature Probing for the Interfacial Thermal Characterization of Epitaxial Graphene on 4H-SiC. *Small* **2011**, *7*, 3324−3333.

(12) Yuan, P.; Wang, R.; Tan, H.; Wang, T.; Wang, X. Energy Transport State Resolved Raman for Probing Interface Energy Transport and Hot Carrier Diffusion in Few-Layered MoS_2. *ACS Photonics* **2017**, *4*, 3115−3129.

(13) Yuan, P.; Tan, H.; Wang, R.; Wang, T.; Wang, X. Very fast hot carrier diffusion in unconstrained MoS_2 on a glass substrate: discovered by picosecond ET-Raman. *RSC Adv.* **2018**, *8*, 12767−12778.
(14) Connell, G. A. N.; Nemanich, R. J.; Tsai, C. C. Interference enhanced Raman scattering from very thin absorbing films. *Appl. Phys. Lett.* **1980**, *36*, 31−33.
(15) Nemanich, R. J.; Tsai, C. C.; Connell, G. A. N. Interference-Enhanced Raman Scattering of Very Thin Titanium and Titanium Oxide Films. *Phys. Rev. Lett.* **1980**, *44*, 273−276.
(16) Ager, J. W., III; Kirk Veirs, D.; Rosenblatt, G. M. Raman intensities and interference effects for thin films adsorbed on metals. *J Chem. Phys.* **1990**, *92*, 2067−2076.
(17) Ramsteiner, M.; Wild, C.; Wagner, J. Interference effects in the Raman scattering intensity from thin films. *Appl. Opt.* **1989**, *28*, 4017−4023.
(18) Yang, Y.; Qiu, T.; Kong, F.; Fan, J.; Ou, H.; Xu, Q.; Chu, P. K. Interference effects on indium tin oxide enhanced Raman scattering. *J. Appl. Phys.* **2012**, *111*, No. 033110.
(19) Craig, R. A.; Exarhos, G. J.; Pawlewicz, W. T.; Williford, R. E. Interference-enhanced Raman scattering from Ti0(2)/Si0(2) multilayers: measurement and theory. *Appl. Opt.* **1987**, *26*, 4193−4197.
(20) Solonenko, D.; Gordan, O. D.; Milekhin, A.; Panholzer, M.; Hingerl, K.; Zahn, D. R. T. Interference-enhanced Raman scattering of F_{16}CuPc thin films. *J. Phys. D: Appl. Phys.* **2016**, *49*, No. 115502.
(21) Wang, Y. Y.; Ni, Z. H.; Shen, Z. X.; Wang, H. M.; Wu, Y. H. Interference enhancement of Raman signal of graphene. *Appl. Phys. Lett.* **2008**, *92*, No. 043121.
(22) Yoon, D.; Moon, H.; Son, Y.-W.; Choi, J. S.; Park, B. H.; Cha, Y. H.; Kim, Y. D.; Cheong, H. Interference effect on Raman spectrum of graphene on SiO_2/Si. *Phys. Rev. B: Condens. Matter Mater. Phys.* **2009**, *80*, No. 125422.
(23) Koh, Y. K.; Bae, M-H.; Cahill, D. G.; Pop, E. Reliably counting atomic planes of few-layer graphene (n > 4). *ACS Nano* **2011**, *5*, 269−274.
(24) Li, X-L.; Qiao, X-F.; Han, W-P.; Lu, Y.; Tan, Q-H.; Liu, X-L.; Tan, P-H. Layer number identification of intrinsic and defective multilayered graphenes up to 100 layers by the Raman mode intensity from substrates. *Nanoscale* **2015**, *7*, 8135−8141.
(25) Li, S-L.; Miyazaki, H.; Song, H.; Kuramochi, H.; Nakaharai, S.; Tsukagoshi, K. Quantitative Raman spectrum and reliable thickness identification for atomic layers on insulating substrates. *ACS Nano* **2012**, *6*, 7381−7388.
(26) Jin, Y.; Rah, Y.; Park, J.; Shim, J.; Yu, K. Rapid and broad-range thickness estimation method of hexagonal boron nitride using Raman spectroscopy and optical microscope. *Appl. Phys. Lett.* **2020**, *116*, No. 081104.
(27) Van Velson, N. V.; Zobeiri, H.; Wang, X. Rigorous prediction of Raman intensity from multi-layer films. *Opt. Express* **2020**, *28*, 35272−35283.
(28) Troparevsky, M. C.; Sabau, A. S.; Lupini, A. R.; Zhang, Z. Transfer-matrix formalism for the calculation of optical response in multilayer systems: from coherent to incoherent interference. *Opt. Express* **2010**, *18*, 24715−24721.
(29) Li, H.; Wu, J.; Yin, Z.; Zhang, H. Preparation and Applications of Mechanically Exfoliated Single-Layer and Multilayer MoS_2 and WSe_2 Nanosheets. *Acc. Chem. Res.* **2014**, *47*, 1067−1075.
(30) Yuan, P.; Liu, J.; Wang, R.; Wang, X. The hot carrier diffusion coefficient of sub-10 nm virgin MoS_2: uncovered by non-contact optical probing. *Nanoscale* **2017**, *9*, 6808−6820.
(31) Beal, A. R.; Hughes, H. P. Kramers-Kronig analysis of the reflectivity spectra of 2H-MoS_2, 2H-$MoSe_2$ and 2H-$MoTe_2$. *J. Phys. C: Solid State Phys.* **1979**, *12*, 881.
(32) Zhao, W.; Ghorannevis, Z.; Amara, K. K.; Pang, J. R.; Toh, M.; Zhang, X.; Kloc, C.; Tan, P. H.; Eda, G. Lattice dynamics in mono- and few-layer sheets of WS_2 and WSe_2. *Nanoscale* **2013**, *5*, 9677−9683.
(33) Lee, C.; Yan, H.; Brus, L. E.; Heinz, T. F.; Hone, J.; Ryu, S. Anomalous Lattice Vibrations of Single- and Few-Layer MoS_2. *ACS Nano* **2010**, *4*, 2695−2700.
(34) Lee, C. H.; McCulloch, W.; Lee, E. W.; Ma, L.; Krishnamoorthy, S.; Hwang, J.; Wu, Y.; Rajan, S. Transferred large area single crystal MoS_2 field effect transistors. *Appl. Phys. Lett.* **2015**, *107*, No. 193503.
(35) Yuan, P.; Wang, R.; Wang, T.; Wang, X.; Xie, Y. Nonmonotonic thickness-dependence of in-plane thermal conductivity of few-layered MoS_2: 2.4 to 37.8 nm. *Phys. Chem. Chem. Phys.* **2018**, *20*, 25752−25761.
(36) Yan, R.; Simpson, J. R.; Bertolazzi, S.; Brivio, J.; Watson, M.; Wu, X.; Kis, A.; Luo, T.; Hight Walker, A. R.; Xing, H. G. Thermal Conductivity of Monolayer Molybdenum Disulfide Obtained from Temperature-Dependent Raman Spectroscopy. *ACS Nano* **2014**, *8*, 986−993.
(37) Liang, L.; Meunier, V. First-principles Raman spectra of MoS_2, WS_2 and their heterostructures. *Nanoscale* **2014**, *6*, 5394−5401.
(38) Wang, R.-p.; Zhou, G.-w.; Liu, Y.-l.; Pan, S.-h.; Zhang, H.-z.; Yu, D.-p.; Zhang, Z. Raman spectral study of silicon nanowires: High-order scattering and phonon confinement effects. *Phys. Rev. B: Condens. Matter Mater. Phys.* **2000**, *61*, 16827−16832.

Recommended by ACS

Ultrafast Electron Microscopy of Nanoscale Charge Dynamics in Semiconductors
Michael Yannai, Ido Kaminer, *et al.*
FEBRUARY 03, 2023
ACS NANO
READ

Plasmonics in Organic Solar Cells: Toward Versatile Applications
Yanglin Zhao, Shenghao Wang, *et al.*
FEBRUARY 09, 2023
ACS APPLIED ELECTRONIC MATERIALS
READ

Real-Time Ratiometric Optical Nanoscale Thermometry
Yongliang Chen, Toan Trong Tran, *et al.*
JANUARY 20, 2023
ACS NANO
READ

High Responsivity in Monolayer MoS_2 Photodetector via Controlled Interfacial Carrier Trapping
Sandhyarani Sahoo, Satyaprakash Sahoo, *et al.*
FEBRUARY 03, 2023
ACS APPLIED ELECTRONIC MATERIALS
READ

Get More Suggestions >

https://doi.org/10.1021/acs.jpcc.2c06353
J. Phys. Chem. C 2023, 127, 2995−3004